

## [NE V] IMAGING OF N49 IN THE LARGE MAGELLANIC CLOUD

CARA E. RAKOWSKI, JOHN C. RAYMOND, AND ANDREW H. SZENTGYORGYI  
Harvard-Smithsonian Center for Astrophysics

submitted July 28, 2006, accepted September 15, 2006

### ABSTRACT

We present sub-arcsecond imaging in [Ne V] of N49, the brightest optical SNR in the LMC. Between the “cool” optical and “hot” X-ray regimes, [Ne V] emission indicates intermediate temperatures for collisionally excited plasmas ( $2\text{--}6 \times 10^5 \text{K}$ ), for which imaging has been extremely limited. We compare the flux in these images to the O VI measured spectroscopically by FUSE in individual apertures and find dereddened line ratios that are reasonably consistent with our predictions for intermediate velocity shocks. The overall luminosity in [Ne V] for the entire remnant is  $1.2 \times 10^{36} \text{ erg s}^{-1}$ , which, given the measured line ratios, implies an overall O VI luminosity of  $1.5 \times 10^{38} \text{ erg s}^{-1}$ . These large radiative losses indicate that this material must have been shocked recently relative to the total lifetime of the remnant. We also explore the complex spatial structure. We find [Ne V] tracing the [O III] emission more closely than it does  $\text{H}\alpha$ , measure significant shifts ( $\sim 0.1 \text{ pc}$ ) between the peaks of different emission lines, and find two orders of magnitude variations in the flux ratios for different filaments across the remnant. These properties as well as the general filamentary character of the optical emission suggest thermally unstable intermediate velocity shocks.

*Subject headings:* supernova remnants:individual(N49) — ISM: structure — shock waves — ultraviolet: ISM

### 1. INTRODUCTION

The ultraviolet (UV) transitions of [Ne V] and O VI probe intermediate temperatures for collisionally ionized plasmas [ $(2\text{--}6) \times 10^5 \text{ K}$ ] inaccessible in the optical or X-ray wavebands. This virtually unexplored temperature range has the most efficient radiative cooling and dominates the radiative losses in supernova remnants (SNRs). Of the potential diagnostics in this regime, the forbidden [Ne V] lines  $\lambda\lambda 3345.8, 3425.9 \text{ \AA}$  are the only bright emission lines accessible from the ground.

While the Far-Ultraviolet Spectroscopic Explorer (FUSE) has successfully provided emission line spectra from intermediate temperature SNR-shocks (Sankrit et al. 2001; Blair et al. 2002; Sankrit & Blair 2002; Sankrit et al. 2004; Korreck et al. 2004) it is not an imaging instrument. Study of the spatial distribution of this intermediate temperature material has been extremely limited. Low spatial resolution ( $\sim 10'$ ) O VI images of the Cygnus Loop and the Vela SNR have been taken above the atmosphere with the High Resolution Emission Line Spectrometer (HIRES) (Rasmussen & Martin 1992) and SPEAR (Spectroscopy of Plasma Evolution from Astrophysical Radiation) (Nishikida et al. 2006) respectively. However, the only high spatial resolution ( $< 1''$ ) image to date of a SNR is the ground-based [Ne V] observation of the Cygnus Loop (Szentgyorgyi et al. 2000). Ground based Fabry-Perot observations of 64 individual sites within the Cygnus Loop in [Ne V] that incorporate spectral information from the tuneable filter were conducted by Sauvageot et al. (1999) but at much lower spatial resolution and hence lower sensitivity to sharp features.

N49 is a good target for exploratory [Ne V] imagery for a number of reasons. It is the brightest optical SNR in the Large Magellanic Cloud (LMC), and hence has a

known distance, is likely to be detectable, and is very well-studied. Previous work has shown evidence of both radiative and hot X-ray emitting shocks. Shull et al. (1985) interpreted this in terms of the evolution of a SNR blast-wave into a complex circumstellar environment sculpted by the progenitor star’s radiation and winds propagating through an existing multi-phase interstellar medium. Given the presence of a much larger existing molecular cloud coincident with the south-east portion of N49 (Hughes et al. 1991), Vancura et al. (1992b) propose a simpler picture in which the temperature and velocity structure seen in N49 are the direct consequence of a Sedov-like blast-wave running into existing large clouds. The filamentary structure of the optical image and the bands seen in the long-slit echelle data would both be the natural consequence of a “rippled sheet” geometry (Hester 1987) of alternating face-on and edge-on shocks as the blast wave envelopes the large clouds. Vancura et al. (1992b) derived a pre-shock density of  $20\text{--}940 \text{ cm}^{-3}$  which they found to be inconsistent with Shull’s model and state that their geometry better explains the structure of the echelle data and the fluxes seen.

### 2. OBSERVATIONS, DATA REDUCTION AND ANALYSIS

Observations of N49 were conducted on 2004 February 16, at the Clay Telescope, one of the twin 6.5m Magellan telescopes at Las Campanas Observatory, Chile ( $-29^\circ$  latitude) using the Raymond and Beverly Sackler Magellan Instant Camera (MagIC). The CCD is a grade 0 SITE 2048 $\times$ 2048 pixel array cooled to a detector temperature of  $-120^\circ \text{ C}$ . The  $24 \mu\text{m}$  pixels each subtend  $0.069''$  and the seeing varied between  $0.''6$  and  $0.''8$ . At 50 kpc to the LMC each pixel corresponds to  $0.0167 \text{ pc}$ . We installed custom [Ne V],  $\text{H}\alpha$ , [O III], and associated continuum filters manufactured by Omega Optical Inc. for our observations (see Table 1). The [Ne V] filter was nar-

TABLE 1  
OBSERVATIONS

Filter	Central $\lambda$ ( $\text{\AA}$ )	FWHM ( $\text{\AA}$ )	Exposure Time (s)	Airmasses	Conversion <sup>a</sup> $\text{erg cm}^{-2} \text{ counts}^{-1}$
[Ne V]	3426	15	1200	1.35,1.38,1.42	4.14E-15
UV continuum	3388	35	1200	1.48,1.54,1.60	
H $\alpha$	6563	46	100	1.33,1.68,1.69,1.70	6.18E-17
red continuum	7130	58	25	1.34,1.72,1.72,1.72	
[O III]	5007	51	50	1.73,1.74,1.74, 1.77,1.79,1.80,1.81	1.14E-16
green continuum	5260	59	20	1.82,1.84,1.86	

<sup>a</sup>Conversion from counts in median combined, continuum subtracted final images

rower and the UV-continuum wider than those used at Whipple Observatory for the study of the Cygnus Loop (Szentgyorgyi et al. 2000).

SNR N49 was at an air mass less than 1.5 for the first half of the night before 4:00UT, during which time we concentrated on the [Ne V] observations. The H $\alpha$  and [O III] images were taken primarily to facilitate comparisons with [Ne V]. Table 1 lists the relevant details of the observations. Routine processing of the data was conducted in IRAF<sup>1</sup> making use of the MagIC package for the specifics of the CCDs. Flat-fielding was performed using twilight sky flats and cosmic-rays were eliminated by median-combining the separate frames. Given the extremely low surface brightness in [Ne V] and the UV continuum, high-frequency electrical noise in the CCD read-out which produced a “herringbone” pattern of 5 to 10 counts could not be ignored. However, due to its slowly temporally varying periodicity it was possible to greatly reduce or even eliminate this signal relative to the diffuse target emission.<sup>2</sup>

Our data were calibrated with observations of the standard star Hiltner 600 taken earlier in the night. The flux as a function of wavelength was taken from LCALIB in IRAF, in particular the flux of Hiltner 600 at 3426 $\text{\AA}$  is  $4.35731 \times 10^{-13} \text{ erg cm}^{-2} \text{ s}^{-1} \text{ \AA}^{-1}$  at the top of the atmosphere. The extinction curves available in IRAF for the Cerro Tololo Inter-American Observatory (CTIO) were used, as they are a reasonable approximation to the extinction at Las Campanas. The filter transmission curves had been measured at Omega Optical Inc., and these data are available at Las Campanas.<sup>3</sup> Over the [Ne V] and UV continuum bandpasses the extinction as a function of zenith distance was well fitted by a third order polynomial, and the filter transmission by a Gaussian. For other filters simple linear or quadratic interpolation was preferred owing to features in the extinction curve or flat tops in the transmission as a function of wavelength. All other aspects of the throughput and detector efficiency were calibrated as a single conversion factor using Hiltner 600. The aggregate efficiency in [Ne V]

was sadly only 4.9%. We estimate that our photometric uncertainty is around 30% based on the mildly variable seeing and the small differences between the calibrated scaling factor for the continuum subtraction and the one which best subtracted the stars. Continuum subtracted images of N49 in H $\alpha$ , [O III], and [Ne V] are displayed separately in Figure 1 and combined into a three-color image in Figure 2: H $\alpha$  (red), [O III] (green), and [Ne V] (blue).

The absolute coordinate system was found by comparison to the U.S. Naval Observatory (USNO) A2.0 catalogue (Monet et al. 1998) using WCSTools (Mink 2002). At least 23 matched stars were identified for each filter with a mean radial offset of 0."367. However the error in the relative positions between the filters is a fraction of a pixel (0.2 – 0.75 pixel) since that is based on registering the same stars in different frames using geomap in IRAF. We note that the X-ray knot identified by Park et al. (2003) is  $\sim 5''$  south of the poorly subtracted star on the western boundary of Figure 2. Park et al. (2003) suggest that this knot is a fragment of ejecta from the SN explosion like those seen in the Vela SNR since it lies outside the apparent boundary of N49 and spectral fits indicate overabundances of O, Si and Fe relative to LMC values. There is nothing at the position of the knot in the [Ne V], H $\alpha$ , or [O III] images that might be identified as cooler emission associated with the X-ray knot.

### 3. DISCUSSION

#### 3.1. Comparison of [Ne V] and O VI

The only information previously available on plasma at a few hundred thousand degrees in N49 comes from measurements of the O VI doublet with the Hopkins Ultraviolet Telescope (HUT) (Vancura et al. 1992b) and FUSE (Blair et al. 2000; Sankrit et al. 2004) UV spectrometers. These spectra provide important line profile information, but they are subject to uncertainties in reddening and in the effects of resonant scattering by O VI ions, both within the emitting plasma (e.g. Long et al. 1992; Raymond et al. 2003) and along the line of sight. There is also a question as to how much of the O VI emission arises from radiative shock waves in the 200  $\text{km s}^{-1}$  range, and how much comes from 300–400  $\text{km s}^{-1}$  non-radiative shocks that produce soft X-rays. Both this question and the uncertainty in the effects of radiative scattering within the emitting gas can be partly answered by examining the way the intensity is distributed within the apertures used for the O VI observation.

The FUSE and HUT apertures are superposed on each of the emission line images of N49 in Figure 1. Table 2

<sup>1</sup> IRAF is distributed by the National Optical Astronomy Observatories, which are operated by the Association of Universities for Research in Astronomy, Inc., under cooperative agreement with the National Science Foundation

<sup>2</sup> A series of “PyRAF” scripts to identify and remove the pattern of electrical noise that combine the IDL and IRAF procedures written by S. Burles and M. Holman, is available on request to C. E. Rakowski. However owing to differences in IRAF and Python distributions and settings, “debugging” is likely to be required.

<sup>3</sup> The actual numbers were extracted from hard-copies of the transmission curves using a stand-alone version of “Dexter” from ADS.

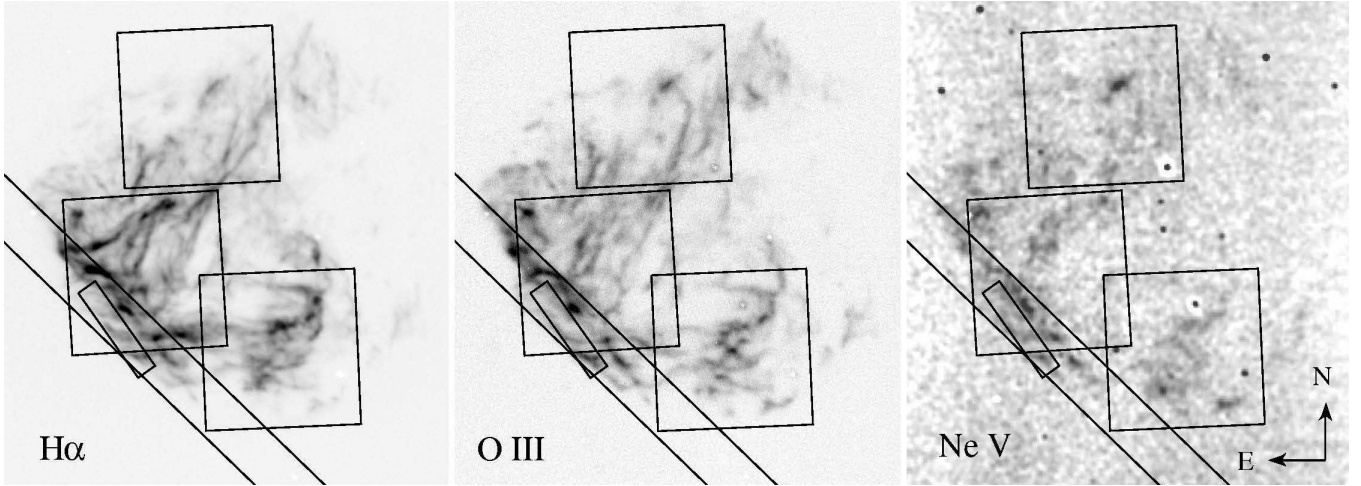


FIG. 1.— Emission-line images of N49  $H\alpha$  (left)  $[O\ III]$  (middle)  $[Ne\ V]$  (right). HUT and FUSE apertures are overlaid. The HUT aperture is the large diagonal swath across the south-east while the  $4'' \times 20''$  diagonal aperture is FUSE C05501. The  $30'' \times 30''$  apertures are C05502, X00502, and C05503 from north to south. The images are linearly scaled over somewhat arbitrary ranges chosen to capture the full dynamic range of each image. The  $[Ne\ V]$  image was first binned by 4 pixels then smoothed with a  $0.828''$  Gaussian kernel.  $H\alpha$  and  $[O\ III]$  were not binned or smoothed.

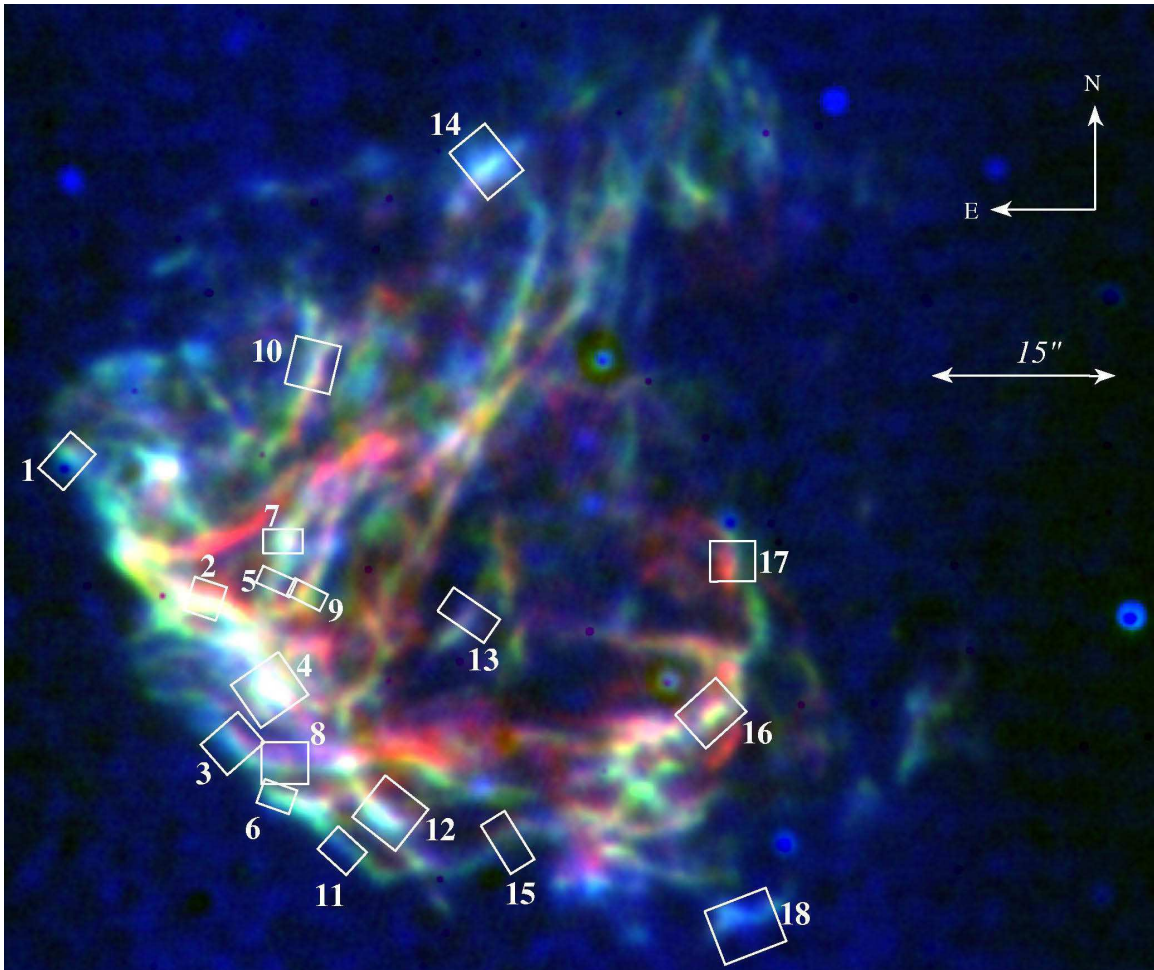


FIG. 2.— Three-color image of N49 in  $H\alpha$  (red),  $[O\ III]$  (green), and  $[Ne\ V]$  (blue). The  $[Ne\ V]$  image was first binned by 4 pixels then smoothed with a  $1.38''$  Gaussian kernel.  $H\alpha$  and  $[O\ III]$  were not binned but were smoothed to  $0.345''$ . Regions from which the filament profiles were extracted are indicated.

TABLE 2  
OBSERVED INTENSITIES ( $10^{-13}$  erg cm $^{-2}$  s $^{-1}$ )

Aperture	[Ne V]	H $\alpha$	[O III]	O VI <sup>a</sup>	WFPC H $\alpha$ <sup>a</sup>
X00502	2.19	210.	64.2	9.9	288.
C05502	1.69	64.4	28.0	6.2	99.0
C05503	1.39	103.	28.8	5.1	126.
C05501	0.34	12.3	6.60	0.96	20.0
HUT	1.30	91.5	33.6	6.0	

<sup>a</sup>Sankrit et al. (2004)

TABLE 3  
DEREDDENED INTENSITIES ( $10^{-13}$  erg cm $^{-2}$  s $^{-1}$ )

Aperture	[Ne V]	H $\alpha$	[O III]	O VI	WFPC H $\alpha$
X00502	13.6	549.	221.	2180.	752.
C05502	10.5	168.	96.4	1360.	258.
C05503	8.66	269.	99.2	1120.	329.
C05501	2.13	32.1	22.7	212.	52.2
HUT	8.10	239.	115.	1320.	

gives the measured intensities in the O VI doublet, along with the intensities in [Ne V]  $\lambda$ 3425, H $\alpha$ , and [O III]  $\lambda$ 5007 measured by integrating over the apertures after masking out a few poorly subtracted stars. Table 2 also gives the H $\alpha$  intensities reported by Sankrit et al. (2004) extracted from an archival HST image.

In Table 3, we give the intensities corrected for a mean reddening  $E(B-V) = 0.37$  as recommended by Vancura et al. (1992b). Vancura et al. (1992b) point out that the reddening is probably not uniform over N49, and that a scatter in the reddening value will introduce a correction factor corresponding to a reduction in  $E(B-V)$ . This is because some fraction of the area within the aperture sees significantly less reddening and contributes a disproportionate amount of flux. Sankrit et al. (2003) assume  $E(B-V) = 0.37$  and that the scatter in  $E(B-V)$  is Gaussian, with a width of 0.14, which reduces the dereddening factor for O VI by a factor of 0.4. Sankrit et al. also estimate that resonance line scattering within the remnant (Long et al. 1992; Raymond et al. 2003) attenuates the O VI flux by about a factor of 1.5, and that scattering in the halo of the LMC decreases the flux by another 20%. The resonance scattering partly compensates for the effect of scatter in  $E(B-V)$ , and the net result is to reduce the corrected flux of O VI by 28%. We include this factor in the fluxes given in Table 3.

The first important comparison is the [Ne V]/O VI ratio. We have computed a model with an updated version of the steady flow shock radiative code of Raymond (1979) and the LMC abundance set of Vancura et al. (1992a). The ratio of O VI to [Ne V] depends only weakly on shock speed in this range, and because the cooling is so heavily dominated by O and Ne at temperatures of  $3\text{--}6 \times 10^5$  K, only the relative abundances of O and Ne come into play. The Vancura et al. LMC abundance set gives O/Ne = 5.0. The major limitation of these models is their neglect of the thermal instabilities that affect shocks faster than about  $150$  km s $^{-1}$  (e.g., Innes 1992; Sutherland et al. 2003). However, the [Ne V] and O VI lines are formed at such similar temperatures that thermal instabilities should not change their ratio significantly. The predicted intensity ratio of [Ne V] to O VI

ranges from 0.0090 to 0.011 for shocks in the 200 to 300 km s $^{-1}$  range. The ratios derived from Table 3 range from 0.0062 to 0.010, in very good agreement with the predictions. This confirms that the reddening and resonance line scattering correction factors of Vancura et al. (1992b) are reliable.

There is one major difference between the O VI and [Ne V] formation temperatures. The emissivity of O VI has a high temperature tail extending to about  $2 \times 10^6$  K, while [Ne V] does not. Hence enhanced O VI might indicate some emission from higher temperature shocks. In fact, the smallest [Ne V]/O VI ratio is in FUSE aperture X00502 where the X-rays are particularly bright. However, the uncertainties in the measurements, the reddening correction, the relative abundances of Ne and O, and the model calculations can easily account for the observed [Ne V]/O VI ratios which lie about 20% below those expected from the radiative shock models. Thus the agreement of the observed flux ratio with the predictions indicates that the bulk of the O VI emission arises from 200–300 km s $^{-1}$  radiative shocks as opposed to the non-radiative shocks that are responsible for producing the X-ray emission from N49.

The second question is the degree of structure of the intermediate temperature gas within the FUSE apertures. The [Ne V] image in Figure 1 shows that in each of the  $30'' \times 30''$  apertures most of the emission comes from filaments a few arcseconds across that cover perhaps 1/3 of the area within the aperture. For example, in the X00502 aperture the three brightest knots covering less than 2% of the aperture contribute 1/8 of the flux. This is what one would expect from the above result that the O VI arises from radiative shocks. When it is possible to obtain an actual O VI image, it should show less contrast than does the [Ne V] image, because scattering will selectively dim the bright, edge-on filaments in resonance lines (Cornett et al. 1992).

The image of N49 gives a total [Ne V] luminosity of the remnant of  $1.2 \times 10^{36}$  erg s $^{-1}$ . From the [Ne V]/O VI ratios, this implies  $L_{OVI} = 1.5 \times 10^{38}$  erg s $^{-1}$ . This is 8 times the X-ray luminosity measured by Long et al. (1981) ( $1.9 \times 10^{37}$  erg s $^{-1}$  from 0.15–4.5 keV). According to the models described above, the O VI luminosity is about 10% of the total energy dissipated by a shock in the 200–300 km s $^{-1}$  range. Thus the luminosity of these intermediate velocity shocks is around  $10^{39}$  erg s $^{-1}$  and in the 6,600 yr estimated lifetime of N49 (Park et al. 2003) they would have radiated  $2 \times 10^{50}$  erg, a significant fraction of the nominal energy of a supernova. According to the shock speed distribution of Vancura et al. (1992a), slower shocks also produce a comparable luminosity. However, if the SNR has recently reached the shell of a bubble produced by the progenitor (Shull et al. 1985) or the dense cloud to the East and South (Hughes et al. 1991) after passing rapidly through low density gas, the age of the shocks could be significantly less than 6,600 yr. Indeed, Park et al. (2003) find a time-scale as short as 100 years based on the ionization state of the X-ray emitting gas in the SE. It is also worth noting that  $L_{OVI}$  is 2.5 times the infrared (IR) luminosity attributed to thermal emission from dust (Graham et al. 1987). Williams et al. (2006) suggest that much of this IR emission comes from emission lines rather than dust, in which case it is produced by intermediate velocity or

slower shocks.

For comparison, estimates of the O VI luminosity of the Cygnus Loop range from  $1.2 \times 10^{36}$  erg s<sup>-1</sup> based on a rocket observation (Rasmussen & Martin 1992) to  $4.6 \times 10^{36}$  erg s<sup>-1</sup> based on a Voyager Ultraviolet Spectrometer observation (Blair et al. 1991). These estimates would be reduced by a factor of 2 for the recent distance estimate of 540 pc (Blair et al. 2005). Thus the O VI luminosity of N49 is 50 to 100 times that of the Cygnus Loop.

Rasmussen & Martin (1992) find that the blast wave can account for the O VI luminosity of the Cygnus Loop, while Vancura et al. (1993) find that the blast wave accounts for only 10 to 15% of the O VI photons. Rasmussen & Martin (1992) point out the overall morphological resemblance between X-ray and O VI emission, while Danforth et al. (2001) discuss a region in the Cygnus Loop where intermediate velocity shocks clearly dominate. The [Ne V] data favor the interpretation of intermediate velocity shocks for N49. The blast wave temperatures in N49 exceed 0.4 keV (Park et al. 2003), which is too high to produce O VI in the high temperature tail. There could in principle be substantial quantities of gas at  $1$  to  $2 \times 10^6$  K whose X-ray emission would be overwhelmed by that of the hotter plasma. Indeed, the detection of [Fe XIV] (Dopita & Mathewson 1979) requires some gas at these temperatures. However, the [Ne V] to O VI ratio derived above shows that this hot gas does not dominate the O VI luminosity.

### 3.2. Spatial distribution and flux ratios of [Ne V], [O III], and H $\alpha$

Vancura et al. (1992b) noted the existence of a rim of [O III] extending outside of the H $\alpha$  emission. They interpreted this as a photoionized precursor. Our images (as well as HST) show that the [O III] emission actually *peaks* outside of H $\alpha$ . However, based on the fraction of [O III] emission in the narrow spike in the [O III] echelle profiles Vancura et al. (1992b) find that the precursor accounts for less than 20% of the [O III] emission. Thus the exterior [O III] filaments must be from the radiative shock itself. This suggests a physical separation between the [O III] and H $\alpha$  in the post-shock gas. In Figure 2 we can identify many exterior and interior filaments where there appears to be a distinct separation between [O III] and H $\alpha$ .

Efficiently radiating intermediate velocity shocks are widely thought to be subject to thermal instabilities for  $v_s > 150$  km s<sup>-1</sup>, but magnetic (Innes 1992) or cosmic-ray (Wagner et al. 2006) pressure can suppress or damp the instability. Large variations in the line fluxes and ratios and wide separations between the emitting regions of different ions may indicate thermally unstable shock conditions. In the non-steady-state radiative shock models of Innes (1992), that include the “cushioning” effect of magnetic pressure support on the collapsing thermally overstable filaments, a peak in [O III] emission ahead of the Balmer line emission was indicative of the presence of secondary shocks. Under the particular shock speed and ambient conditions they chose ( $V_S = 175$  km s<sup>-1</sup>,  $n_0 = 1$  cm<sup>-3</sup>,  $B_0 = 3\mu$ G) the separations between peaks are typically  $4\text{--}7'' \times (D/1 \text{ kpc})^{-1}$  but can at times be as large as  $20'' \times (D/1 \text{ kpc})^{-1}$ . Innes (1992) also finds that the crossings of multiple secondary shocks result in relatively short-term time variations in

both the line-intensities and line-ratios with line-ratio fluctuations of greater than a factor of 20. They further predict an [O III] photoionization precursor extending  $45'' \times (D/1 \text{ kpc})^{-1}$  with intensities 15–20% of the peak [O III] emission which can account for the echelle spectra.

At the distance to the LMC the calculations of Innes (1992) translate into separations as large as  $0.4''$ . However the densities required to explain the flux are at least a factor of 20 higher than modeled by Innes (1992) while the lower LMC abundances will increase the cooling time by a factor of 3. Thus we would expect the separations to be a factor of 6 smaller than the predictions of Innes (1992) unless there was significantly more pressure support either from a higher magnetic field or cosmic-rays.

To quantify the separations and flux variations, 18 regions were chosen along “straight” sections of filaments where relatively clean profiles could be extracted in each filter. These include the clearest examples of spatial separations plus a few profiles to represent the more typical cases where the peaks in all bands essentially coincide. The profiles, labeled “1” to “18” from east to west in Figure 2, were fit with Gaussians to determine the peak amplitude, position and full-width-half-maximum (FWHM) of the filament in each band above a flat background level. Of these, 13 profiles were well-characterized by this simple model, while others with wider profiles or that simply reached a plateau were not. Selected profiles are shown in Figure 3 and plots of the relative distances between peaks, the ratios of the integrated fluxes, and the relative widths of the filaments are shown in Figure 4. From this investigation we find the following:

- Any given ratio of fluxes [Ne V]/ H $\alpha$ , [Ne V]/ [O III], or [O III]/ H $\alpha$  varies over 2 orders of magnitude (as measured by the parameters of the Gaussian fits), with the highest [Ne V]/ H $\alpha$  ratio occurring in region 18 at the far southwestern edge of the remnant.
- In most of the regions the widths of the filament in all bands are similar, but in regions 1, 6, 7, 11, 12, and 18 the [Ne V] emission appears more extended. Region 11 (along the southeast bright portion) in particular shows a wider profile in [Ne V] extending ahead of the other two.
- Measured separations between the peak flux in [O III] and H $\alpha$  are as large as 0.15 pc ( $0.62''$ ) in the extreme cases of regions 3 and 17, and at least 11 regions show separations larger than 0.05 pc ( $0.2''$ ). In over half of the regions the peak in [Ne V] lies between the other two, closer to the peak in [O III]. The exceptions are regions 2 and 12 where [Ne V] and H $\alpha$  essentially coincide, and 5, 6, 11 and 14 where [Ne V] leads [O III] by as much as 0.04 pc ( $0.17''$ ).

The flux ratio variations are in line with the idea of different filaments being at different stages of thermal instability. In fact, we find that steady flow shock models cannot explain [O III]/H $\alpha$  > 2/3 or [Ne V]/[O III] > 1/4 for LMC abundances, both of which are seen. We also expect that the [O III] and H $\alpha$  emission from cooler,

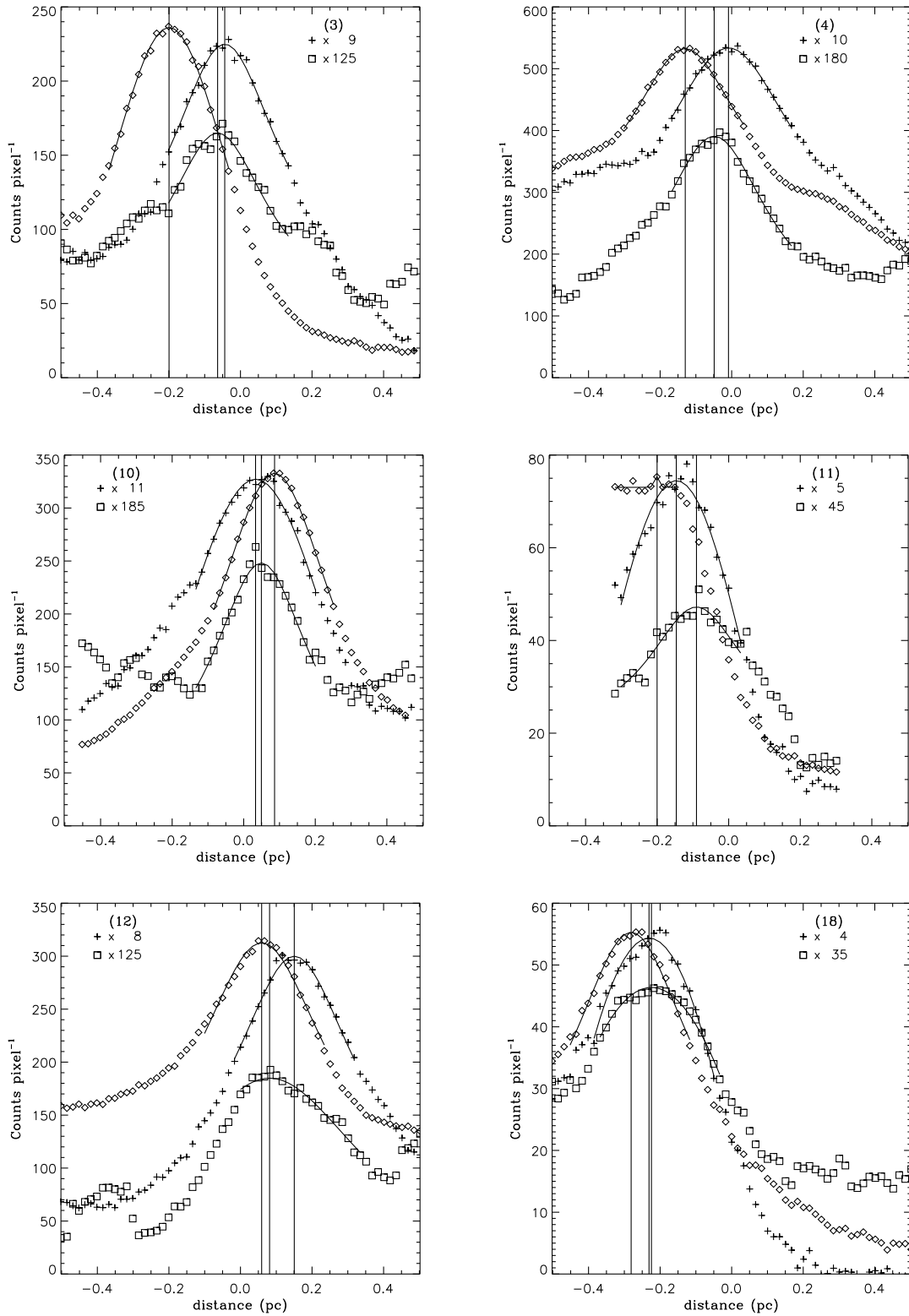


FIG. 3.— Intensity profiles across selected filaments,  $H\alpha$  (diamonds),  $[O III]$  (pluses), and  $[Ne V]$  (squares). Six profiles 3,4,10,11,12, and 18, were chosen to demonstrate the range of properties seen among the 18 extracted. The fainter  $[O III]$  and  $[Ne V]$  have been multiplied by the factors shown in each plot. All profiles were extracted from the original unsmoothed, unbinned data and are displayed in terms of the average counts pixel<sup>-1</sup> versus the distance in pc to give a better sense of the statistics. Conversion factors from counts to flux and the exposure times are as given in Table 1.

compressed gas should be narrower than the [Ne V] filaments which trace the  $2\text{--}6 \times 10^5 \text{K}$  shocked gas. We do see evidence for this in some places. The positions of peak brightness in [O III],  $\text{H}\alpha$ , and [Ne V] are often significantly offset from one another by distances of order 0.1 pc similar to the predictions for a much lower density, solar abundance plasma (Innes 1992). Thus if the flux ratios and separations in N49 are to be explained by thermal instability significant magnetic or cosmic-ray pressure support would be required to slow the progress of the instability.

The filamentary nature itself is evocative of thermally unstable shocks such as the “ribbons of high density” in the simulations of Blondin et al. (1998). The structures in N49 appear similar in scale and curvature to the late times of their high ambient density simulation (Blondin et al. 1998, Figure 11). Quantitatively an actual filamentary structure of condensed ribbons is not required because the surface brightness contrast between the filaments and the diffuse emission (factors of 5–10 in [O III]) is still consistent with a rippled sheet geometry (Hester 1987). However the similarities are highly suggestive.

#### 4. SUMMARY

N49 exhibits an extremely bright complex structure in [Ne V]. The radiative losses alone imply a recent interaction with dense material relative to the age of the remnant. The ratios of [Ne V] to O VI emission, which both occur at  $2\text{--}6 \times 10^5 \text{K}$ , are consistent with emission from  $200\text{--}300 \text{ km s}^{-1}$  shocks, confirming the dereddening relation of Sankrit et al. (2003) and implying that most of the O VI emission arises from  $200\text{--}300 \text{ km s}^{-1}$  radiative shocks. For [Ne V], [O III], and  $\text{H}\alpha$ , which occur at decreasing temperatures post-shock, we find  $\sim 0.1$  pc separations between the peaks of their emission in individual filaments and a factor of 100 variation in their relative fluxes, including a number of places where the [O III]/ $\text{H}\alpha$  or [Ne V]/[O III] flux ratios are higher than allowed by steady flow shock models at LMC abundances. These properties are consistent with the presence of thermal instabilities, but at the densities implied by the total flux, additional magnetic or cosmic-ray pressure would be required.

Thermal instabilities have been almost universally predicted to occur in radiative shocks above  $v_s > 150 \text{ km s}^{-1}$ , however observational evidence for them has been severely lacking. Density fluctuations in the pre-shock medium can mask or mimic the effects of thermal instability and it can be difficult to distinguish between different departures from steady-flow. For instance in the Cygnus Loop, high [O III]/ $\text{H}\alpha$  flux ratios are interpreted as evidence for a truncated or incomplete recombination zone behind a recent shock interaction (Raymond et al. 1980, 1988). In that particular region it seems unlikely that thermal instabilities have taken hold given the smooth variation of properties over such an extended thin structure (Raymond et al. 1988). In the slightly faster shocks of N49, on the other hand, we are interpreting the variability over the entire remnant as snapshots of different stages in thermally unstable shocks. In N49, the spatial separation and large variability are the keys to interpreting the non-steady-flow flux ratios. However, without additional magnetic or cosmic ray pressure these structures would have been unresolvable.

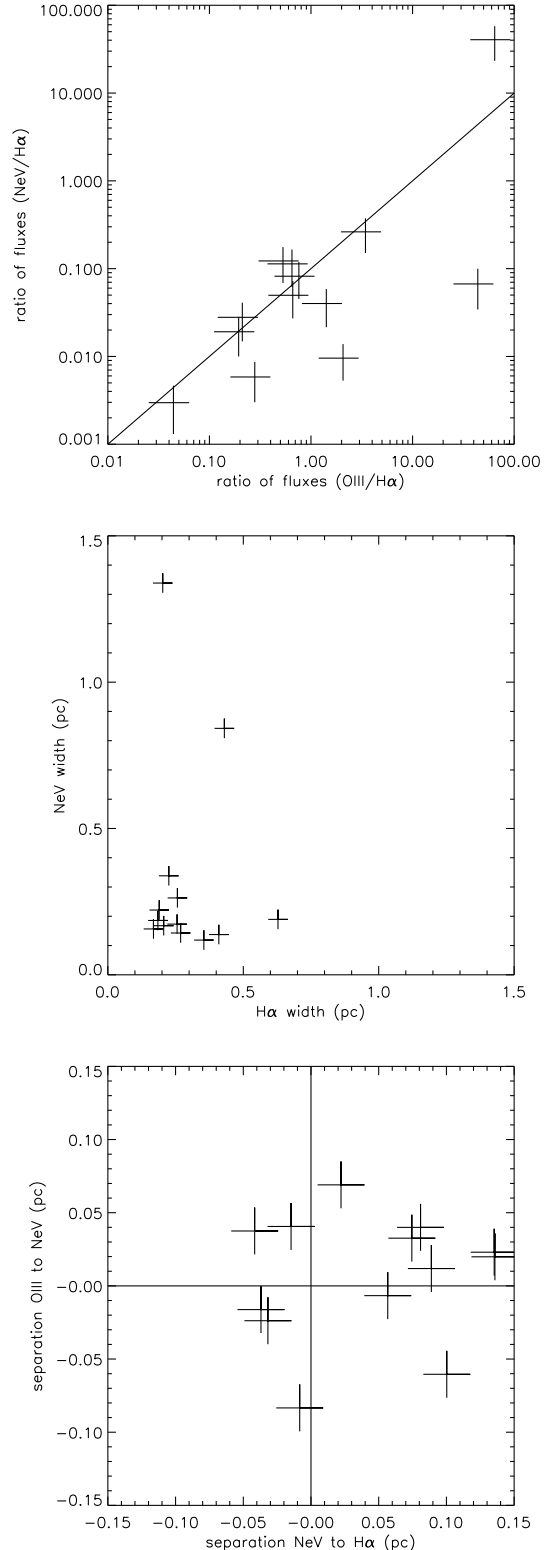


FIG. 4.— Gaussian line-profile parameters for the selected regions. (a) Flux ratios of [Ne V]/ $\text{H}\alpha$  vs. [O III]/ $\text{H}\alpha$  measured by the area under the Gaussian and dereddened. (b) Width in pc of [Ne V] vs.  $\text{H}\alpha$ . (c) Separation in pc, between the peaks of emission, [O III] to [Ne V] vs. [Ne V] to  $\text{H}\alpha$ . Overplotted in (a) is the line [Ne V]/[O III] = 0.1. Only regions for which a Gaussian line-profile captured the peak position and width were included in these plots. Errors shown are based on (a) 30% error in calibration and the square-root of the number of counts, (b)  $\pm 2$  pixels, and (c)  $\pm 1$  pixel.

The authors would like to thank Scott Burles for the use of his IDL routine to identify the “herring-bone” electrical noise using a one-dimensional fast-fourier-transform and Matthew Holman for the valuable observation that in MagIC the pattern of electrical noise

is mirrored over each of the four chips allowing the diffuse source emission to be removed prior to identifying the pattern. C.E.R. was supported during this work by NASA Grant NAG5-9281.

*Facilities:* Magellan:Clay (MagIC)

## REFERENCES

- Blair, W. P., Long, K. S., Vancura, O., & Holberg, J. B. 1991, *ApJ*, 374, 202
- Blair, W. P., Sankrit, R., & Raymond, J. C. 2005, *AJ*, 129, 2268
- Blair, W. P., Sankrit, R., Shelton, R., Sembach, K. R., Moos, H. W., Raymond, J. C., York, D. G., Feldman, P. D., Chayer, P., Murphy, E. M., Sahnou, D. J., & Wilkinson, E. 2000, *ApJ*, 538, L61
- Blair, W. P., Sankrit, R., & Tulin, S. 2002, *ApJS*, 140, 367
- Blondin, J. M., Wright, E. B., Borkowski, K. J., & Reynolds, S. P. 1998, *ApJ*, 500, 342
- Cornett, R. H., Jenkins, E. B., Bohlin, R. C., Cheng, K.-P., Gull, T. R., O’Connell, R. W., Parker, R. A. R., Roberts, M. S., Smith, A. M., Smith, E. P., & Stecher, T. P. 1992, *ApJ*, 395, L9
- Danforth, C. W., Blair, W. P., & Raymond, J. C. 2001, *AJ*, 122, 938
- Dopita, M. A. & Mathewson, D. S. 1979, *ApJ*, 231, L147
- Graham, J. R., Evans, A., Albinson, J. S., Bode, M. F., & Meikle, W. P. S. 1987, *ApJ*, 319, 126
- Hester, J. J. 1987, *ApJ*, 314, 187
- Hughes, J. P., Bronfman, L., & Nyman, L. 1991, in *Supernovae*, ed. S. E. Woosley (Springer-Verlag, New York), 679
- Innes, D. E. 1992, *A&A*, 256, 660
- Korreck, K. E., Raymond, J. C., Zurbuchen, T. H., & Ghavamian, P. 2004, *ApJ*, 615, 280
- Long, K. S., Blair, W. P., Vancura, O., Bowers, C. W., Davidsen, A. F., & Raymond, J. C. 1992, *ApJ*, 400, 214
- Long, K. S., Helfand, D. J., & Grabelsky, D. A. 1981, *ApJ*, 248, 925
- Mink, D. J. 2002, in *ASP Conf. Ser. 281: Astronomical Data Analysis Software and Systems XI*, ed. D. A. Bohlender, D. Durand, & T. H. Handley, 169
- Monet, D. B. A., Canzian, B., Dahn, C., Guetter, H., Harris, H., Henden, A., Levine, S., Luginbuhl, C., Monet, A. K. B., Rhodes, A., Riepe, B., Sell, S., Stone, R., Vrba, F., & Walker, R. 1998, 1252
- Nishikida, K., Edelstein, J., Korpela, E. J., Sankrit, R., Feuerstein, W. M., Min, K. W., Shinn, J.-H., Lee, D.-H., Yuk, I.-S., Jin, H., & Seon, K.-I. 2006, *ApJ*, 644, L171
- Park, S., Burrows, D. N., Garmire, G. P., Nousek, J. A., Hughes, J. P., & Williams, R. M. 2003, *ApJ*, 586, 210
- Rasmussen, A. & Martin, C. 1992, *ApJ*, 396, L103
- Raymond, J. C. 1979, *ApJS*, 39, 1
- Raymond, J. C., Hartmann, L., Black, J. H., Dupree, A. K., & Wolff, R. S. 1980, *ApJ*, 238, 881
- Raymond, J. C., Hester, J. J., Cox, D., Blair, W. P., Fesen, R. A., & Gull, T. R. 1988, *ApJ*, 324, 869
- Raymond, J. C., Ghavamian, P., Sankrit, R., Blair, W. P., & Curiel, S. 2003, *ApJ*, 584, 770
- Sankrit, R. & Blair, W. P. 2002, *ApJ*, 565, 297
- Sankrit, R., Blair, W. P., & Raymond, J. C. 2003, *ApJ*, 589, 242
- 2004, *AJ*, 128, 1615
- Sankrit, R., Shelton, R. L., Blair, W. P., Sembach, K. R., & Jenkins, E. B. 2001, *ApJ*, 549, 416
- Sauvageot, J. L., Decourchelle, A., & Bohigas, J. 1999, *A&A*, 351, 669
- Shull, Jr., P., Dyson, J. E., Kahn, F. D., & West, K. A. 1985, *MNRAS*, 212, 799
- Sutherland, R. S., Bicknell, G. V., & Dopita, M. A. 2003, *ApJ*, 591, 238
- Szentgyorgyi, A. H., Raymond, J. C., Hester, J. J., & Curiel, S. 2000, *ApJ*, 529, 279
- Vancura, O., Blair, W. P., Long, K. S., Davidsen, A. F., Bowers, C. W., Dixon, W. V. D., Durrance, S. T., Feldman, P. D., Ferguson, H. C., Henry, R. C., Kimble, R. A., Kriss, G. A., Kruk, J. W., & Moos, H. W. 1992a, *ApJ*, 401, 220
- Vancura, O., Blair, W. P., Long, K. S., & Raymond, J. C. 1992b, *ApJ*, 394, 158
- Vancura, O., Blair, W. P., Long, K. S., Raymond, J. C., & Holberg, J. B. 1993, *ApJ*, 417, 663
- Wagner, A. Y., Falle, S. A. E. G., Hartquist, T. W., & Pittard, J. M. 2006, *A&A*, 452, 763
- Williams, R. M., Chu, Y. ., & Gruendl, R. 2006, *AJ*, in press